European Journal of Wood and Wood Products (2020) 78:321–331
https://doi.org/10.1007/s00107-020-01494-0

ORIGINAL

# Experimental analysis of the forming behavior of ash wood veneer with nonwoven backings

David Zerbst[1] · Emanuela Affronti[2] · Thomas Gereke[3] · Beate Buchelt[4] · Sebastian Clauß[1] · Marion Merklein[2] · Chokri Cherif[3]

Received: 19 March 2019 / Published online: 15 February 2020


**Abstract**
In the present study, the forming behavior of veneer with nonwoven backings was analyzed. The paper contributes to the lack of data on numerical predictions of the formability of veneers for the manufacturing of automotive trim parts. Tensile and shear tests were carried out at normal climate conditions and after water immersion to obtain material parameters for a transverse isotropic material description. The Tsai Wu failure criterion was applied to the estimation of strength under different stress combinations. Analysis of the directional deep drawing capacity of the veneer laminate was done by the Nakajima test. Stress states from biaxial to uniaxial were induced into the material depending on the geometry of the sample. Strains were evaluated locally until material failure using the digital image correlation method. Major strain was defined in the direction perpendicular to the grain. Increasing major strain was found from biaxial to uniaxial stress states. Highest strain limits were found for wet veneers tested with heated forming tools. Cracks occurred in the early wood zone for all geometries and propagated in the direction parallel to the grain. Generally, the Nakajima test is suitable for the evaluation of the formability of veneer laminate sheets. The presented data and, in general, the suggested experimental program can be used for the development and validation of veneer laminate material models for forming simulations.

## 1 Introduction

Decorative wooden trim parts in car interiors are basically composed of a base support made of plastic and a thin veneer surface finished with a coating. Thereby, the veneer surface is made of a veneer laminate (VL): a veneer with a nonwoven backing. The textile reinforcement is applied to support the very thin and brittle wood veneer, to improve its pliability and minimize cracking (Dexle and Wiblishauser 1999). In the production process, the VL is first formed into the target geometry using metallic forming tools. Afterwards, the plastic support structure is attached with an injection molding process. The forming of veneers has limitations because of the anisotropic and inhomogeneous environment-dependent nature of wood. The conception of a stable forming process and the prediction of the formability of a given geometry is difficult due to these characteristics.

Many parameters influence the mechanical properties of VL regarding the forming process. The most influencing factors are the moisture content and the forming temperature. An overview of thermo-hydro-mechanical processing of wood is given by Navi and Sandberg (2012). The slicing technique (Pfriem and Buchelt 2011) and, in the case of the VL, the fabric and the adhesive affect the compounds formability (Buchelt and Wagenführ 2010; Zerbst and Clauss 2018).

Veneer mechanics were characterized in a few studies using 2D analyses such as tensile tests. Bellair (2013) investigated and analyzed the material properties of beech wood veneer as input for computational modelling of the forming process. Based on this work, Dietzel et al. (2016) carried out tensile tests with strain field measurements on walnut burl veneers in clear and textile layered variants under different

✉ David Zerbst
david.zerbst@daimler.com

✉ Thomas Gereke
Thomas.gereke@tu-dresden.de

[1] Mercedes Benz Cars RD, Sindelfingen, Germany

[2] Institute of Manufacturing Technology, Friedrich-Alexander-Universität Erlangen-Nürnberg, Nuremberg, Germany

[3] Institute of Textile Machinery and High Performance Material Technology, Technische Universität Dresden, Dresden, Germany

[4] Institute of Natural Materials Technology, Technische Universität Dresden, Dresden, Germany

climate conditions. They also derived a finite element model based on multilayered shell elements.

Previous papers regarding the 3D deformation behavior of veneers only considered one stress state. Furthermore, these tests were not equipped with optical measurement systems for investigations of local material properties. Wagenführ et al. (2006) applied a customized Erichsen cupping test. A hemisphere was punched into circular veneer samples. They compared the deflection of the veneers until failure for different wood species and sheet thicknesses under standard climate conditions. The highest deformation was obtained with sycamore maple. The worst forming results were determined for American walnut, which was traced back to a high ratio of anisotropy. Fekiac et al. (2016) found an increasing deepening of circular veneer samples with increasing moisture content and steam pre-treatment. The best formability was found for birch veneer, whereas beech veneer and ash veneer showed lower but almost similar forming behavior. Clauß et al. (2014) generally characterized common ash wood mechanics.

Other works dealt with the question of improving the forming properties by different chemical, physical and biological treatments (Goswami et al. 2008; Herold and Pfriem 2013; Fekiač et al. 2014; Franke et al. 2018). For practical applications, these proposals are not satisfyingly verified, because they were not combined with varying moisture and temperature during testing and solely conducted with pure veneer sheets.

Basic forming technologies of veneer products are discussed by Grabner et al. (2016). In the automotive industry, the forming of veneers is usually done in a pressing tool with different mechanisms for the sheet fixation. The tools are heated to temperatures of around 140 °C. The VL sheets are wetted before forming. Due to the various structures of wooden materials, the forming process is different for each VL sheet, i.e. cracks, wrinkles and distortions can occur. Thus, the manufacturing is mainly based on hands-on experiences of the workers, who apply water locally on the sheets. For the development of feasible trim parts with wood surfaces and the conceptual design of a stable forming process, fundamental understanding of the material forming behavior is needed. Numerical simulations can help to analyze and understand the material and process parameters during forming. Predictions of the formability with numerical simulation tools require measurements of directional material parameters and analysis of material failure. While sheet metal forming has been extensively studied, characterized and implemented into computational models, the database for wood VL forming processes is not sufficient.

The aim of the present study is to provide a full set of experimental data from 2D standard tests, using a tensile and shear test and 3D forming analyses using the Nakajima test. In the field of sheet metal forming, the Nakajima test is used as a standard test to determine the forming limit of a material, under varying stress combinations (Nakajima et al. 1968). Furthermore, it can be used for the evaluation of simulation results or directly as input in some material models. In this study, this method is transferred to characterize the 3D forming behavior of VL sheets under applied moisture and temperature conditions.

## 2 Experimental methods

### 2.1 Derivation of the experimental program

Basic structural-mechanical modelling requires the determination of elastic constants and strength parameters in the main material directions. A linear-elastic material description according to Hooke´s law in orthotropic formulation is given as

$$\begin{pmatrix} \varepsilon_{11} \\ \varepsilon_{22} \\ \varepsilon_{33} \\ \gamma_{12} \\ \gamma_{23} \\ \gamma_{31} \end{pmatrix} = \begin{bmatrix} \frac{1}{E_1} & -\frac{\nu_{21}}{E_2} & -\frac{\nu_{31}}{E_3} & 0 & 0 & 0 \\ -\frac{\nu_{12}}{E_1} & \frac{1}{E_2} & -\frac{\nu_{32}}{E_3} & 0 & 0 & 0 \\ -\frac{\nu_{13}}{E_1} & -\frac{\nu_{23}}{E_2} & \frac{1}{E_3} & 0 & 0 & 0 \\ 0 & 0 & 0 & \frac{1}{G_{12}} & 0 & 0 \\ 0 & 0 & 0 & 0 & \frac{1}{G_{23}} & 0 \\ 0 & 0 & 0 & 0 & 0 & \frac{1}{G_{13}} \end{bmatrix} \begin{pmatrix} \sigma_{11} \\ \sigma_{22} \\ \sigma_{33} \\ \tau_{12} \\ \tau_{23} \\ \tau_{31} \end{pmatrix} \tag{1}$$

where $\varepsilon_{ii}$ are normal strains, $\gamma_{ij}$ are shear strains, $\sigma_{ii}$ are normal stresses, $\tau_{ij}$ are shear stresses, $E_i$ are Young's moduli, $G_{ij}$ shear moduli, and $\nu_{ij}$ are Poisson's ratios. Symmetry is given by

$$\frac{\nu_{12}}{E_1} = \frac{\nu_{21}}{E_2}; \frac{\nu_{13}}{E_1} = \frac{\nu_{31}}{E_3}; \frac{\nu_{23}}{E_2} = \frac{\nu_{32}}{E_3} \tag{2}$$

The three growth related material directions of wood are defined in the longitudinal (1) direction of the tree as well as in the radial (2) and tangential (3) directions of the growth rings. The Poisson's ratio $\nu_{ij}$ is the negative ratio of lateral strain $\nu_j$ and the principal strain in the load direction $\varepsilon_i$ as

$$\nu_{ij} = -\frac{\varepsilon_j}{\varepsilon_i}; \quad i,j = 1,2,3; i \neq j \tag{3}$$

For veneers and especially the VL, the grain angle in the 23-plane differs widely and is hard to differentiate. Therefore, the material is assumed to be transverse isotropic with material directions parallel and perpendicular to the grain. Under the assumption of isotropic plane 23, the compliance tensor reduces as follows

$$E_2 = E_3, G_{12} = G_{13},\ \nu_{12} = \nu_{13}, \nu_{23} = \nu_{32} \tag{4}$$

and the relation

$$G_{23} = \frac{E_2}{2\left(1+\nu_{23}\right)} \tag{5}$$

Following these considerations, five independent constants have to be determined from measurements for a full linear elastic material description: $E_1$, $E_2$, $\nu_{12}$, $G_{12}$, $G_{23}$.

## 2.2 Tsai–Wu failure surface

To characterize the 3D forming limits of VL, a failure hypothesis is needed to capture strength conditions under different stress states. Based on strength values from standard testing, a brittle failure criterion can be applied. In a comparison of different failure models, Mascia and Simoni (2013) found a good agreement of the Tsai–Wu failure criterion with results from biaxial compression tests of two Brazilian wood species. Following this work, the Tsai–Wu criterion was applied in this study to describe multidimensional strength of the VL. The Tsai–Wu equation describes the interaction of different stress components and their effects on strength with an ellipsoid function (Tsai and Wu 1971). The function is given as

$$F_i \cdot \sigma_i + F_{ij} \cdot \sigma_i \sigma_j = 1 \ \ i,j = 1,2 \tag{6}$$

where $F_i$ and $F_{ij}$ are the strength tensors and $\sigma_i$ and $\sigma_j$ are the scalar stress components. Under the assumption of plane stress for VL sheets the expression reduces to:

$$F_1 \cdot \sigma_1 + F_2 \cdot \sigma_2 + F_{11} \cdot \sigma_1^2 + F_{22} \cdot \sigma_2^2 + 2F_{12} \cdot \sigma_1 \sigma_2 + F_{44} \cdot \tau_{12}^2 = 1 \tag{7}$$

The linear term specifies the strength limits in the material directions and the quadratic terms create an ellipsoidal surface in the principal stress space. A material can withdraw all stress combinations fulfilling the condition $f\left(\sigma_{ij}\right) < 1$. The strength coefficients can be calculated with experimentally determined strength parameters in tension ($f_{ti}$), compression ($f_{ci}$) and shear ($f_{sij}$) as follows:

$$\begin{aligned}
F_1 &= \frac{1}{f_{t1}} - \frac{1}{f_{c1}}, \\
F_2 &= \frac{1}{f_{t2}} - \frac{1}{f_{c2}}, \\
F_{11} &= \frac{1}{f_{t1} \cdot f_{c1}}, \\
F_{22} &= \frac{1}{f_{t2} \cdot f_{c2}}, \\
F_{44} &= \frac{1}{f_{s12}}, \\
F_{12} &= K\sqrt{F_{11} \cdot F_{22}}
\end{aligned} \tag{8}$$

The interaction term $F_{12}$ adjusts the rotation of the failure surface around the shear axis. Keeping the boundary condition of $-1 \le K \le 1$ ensures a closed ellipsoidal surface. Factor $K$ has to be calibrated from biaxial measurements. Failure surfaces of the VL were created with GNU Octave mathematic code.

## 2.3 Material

For the characterization of the sheet forming process, ash wood veneer (*Fraxinus excelsior* L.) laminated with a cellulose based nonwoven fabric on the backside was chosen. This material is frequently used as decorative surface in automotive interior. Veneer and nonwoven fabric were laminated using a phenol–formaldehyde-based adhesive. The nonwoven fabric has a preferred orientation of the fibers in the direction of production. In the laminate, fiber directions of veneer and fabric were oriented parallel to each other. The laminate was calibrated to a thickness of 0.5 mm, where the veneer was 0.3 mm thick.

## 2.4 Moisture pretreatment

Material testing under realistic industrial forming conditions is challenging because moisture content and temperature inside of the material vary during the forming process. In laboratory studies, standardized conditions are used. Srinivasan et al. (2007) and Chanda and Bhattacharyya (2018) stated a water bath of 60 s with 60–80 °C for a moisture content between 40 and 50% as optimal condition to avoid spring back and spring forward effects. These effects are not relevant for the manufacturing of formed surfaces of trim parts. In industrial production, the final shape of those surfaces is fixed with a layer of plastic, which is applied in a subsequent injection-molding step. In a process with heated forming of 140 °C, a lot of water vaporizes from the time of inserting the VL until closure of the forming tools. This leakage is even greater in the Nakajima test with an open die (Fig. 1). Hence, in addition to normal climate conditions (20 °C/65% RH), a high moisture content above the

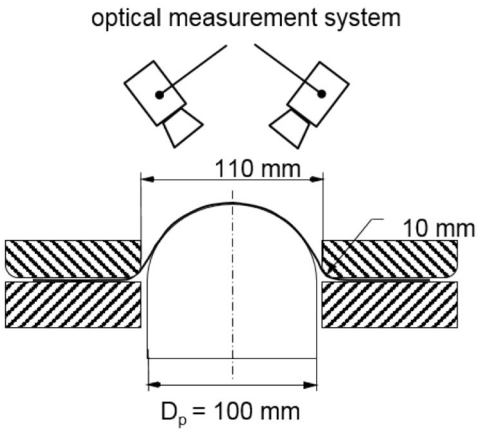


**Fig. 1** Nakajima test setup

fiber saturation point was chosen for the material tests. The presence of free water should maintain a high level of moisture inside the samples during forming. Therefore, samples were put into water at 20 °C for 1 h. The samples achieved a moisture content of around 52% (Fig. 2). At normal climate conditions, the moisture content of the VL was 7%, and the average density was 780 kg/m$^3$.

## 2.5 2D testing

Young's modulus, tensile strength and ultimate strain at failure were derived from tensile tests. The tests were performed with a standard testing device (Inspekt 10, Hegewald & Peschke, Nossen, Germany) parallel and perpendicular to the grain. The sample geometry was $10 \times 120$ mm$^2$ with a section of observation of $10 \times 80$ mm$^2$ between the clamping jaws. Tensile strain and lateral strain were calculated based on deformations recorded with an optical measurement system (Video extensometer ME 46 of Messphysik, Fürstenfeld, Austria). Furthermore, the in plane shear modulus and shear strength were determined from a shear frame test with samples of $10 \times 10$ mm$^2$. The shear test was carried out according to Krüger et al. (2018). The kinematics of the used shear frame setup were limited to avoid contact between the clamping jaws. Both tests were performed under normal climate conditions and after water immersion of 1 h. The testing velocity was 1 mm/min. 20 replicates were conducted for the determination of each parameter.

## 2.6 Nakajima test

In the field of sheet metal forming, the Nakajima test is used as a standard test to characterize the forming limit of a material. Furthermore, it can be used for the evaluation of simulation results or directly as input in some material models. In this study, the test was applied to characterize the 3D forming behavior of VL. The Nakajima test was carried out following DIN EN ISO 12004-2 (2009). The Nakajima setup at the Institute of Manufacturing Technology at the Friedrich-Alexander University Erlangen-Nuremberg is an in-house development and is depicted in Fig. 1. The blank holder and the die allow a force-controlled sheet clamping. The hemispherical punch has a diameter of 100 mm. The constant vertical punch movement forms the sheet until fracture occurs. The test history was recorded with the optical measurement system Aramis (gom GmbH, Germany).

Sample geometries are shown in Fig. 3. Following the standard, different sample geometries were used for the determination of the forming limit under different strain paths. A full circular geometry with a diameter of 245 mm was used to induce a biaxial stress state. A geometry with a small width of the parallel shaft of 30 mm was used to induce almost uniaxial strain. Two geometries with a width of 70 mm and 125 mm induced a stress state in-between uniaxial and biaxial. The significant structural difference between VL and metals suggests that the different geometries will give only small differences in the strain path due

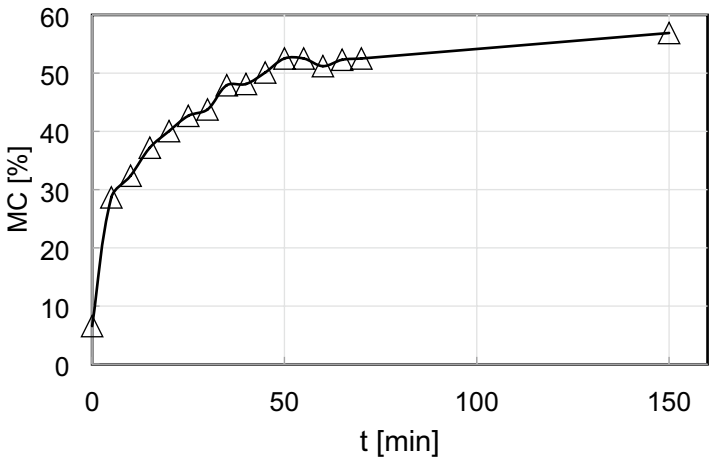


**Fig. 2** Moisture content (MC) of one tensile sample as a function of time of water immersion (t)

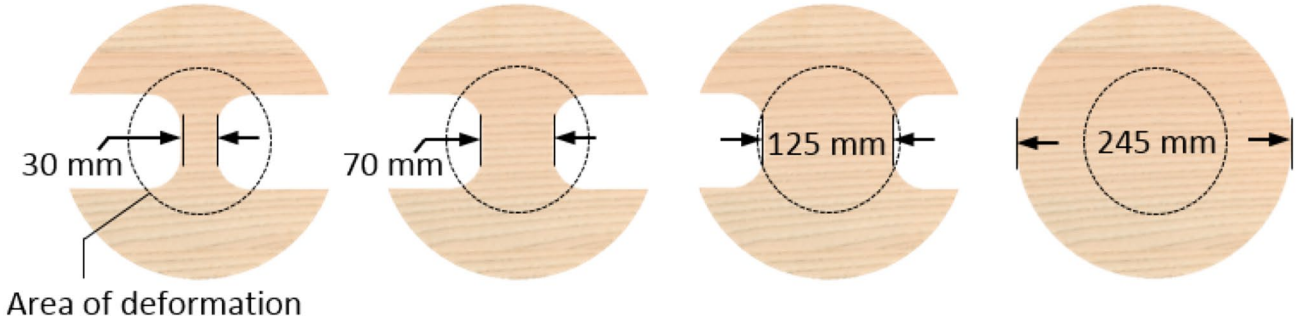


**Fig. 3** Sample geometries (from left to right: S30, S70, S125, S245)

to the high anisotropy with respect to the grain orientation. However, due to the lack of literature data regarding the formability of veneers, in the present study, several geometries were tested and compared. The geometries were cut perpendicular to the grain direction. For each geometry, 10 specimens were tested and evaluated.

The used Nakajima testing device is designed for measurements of forming properties of sheet metals. Therefore, it is not installed in a controlled climate chamber, as it is commonly done for the testing of wood-based materials. Hence, the formability of the VL was analyzed at room climate (climate R) and after water immersion of 1 h (climate W), as it was done in the standard tests. In a third state, water-immersed samples were tested when the punch, the die and the holder of the Nakajima testing device were heated to a constant temperature of 140 °C (climate W + H). This represents the process conditions of heated forming tools in the industrial forming process.

The punch was moved with a constant velocity of 90 mm/min. To minimize the friction between punch and specimen, a PTFE-foil was used as intermediate layer. A stochastic pattern of white and black spray paint was applied on the surface of the samples for the evaluation of the optical measurement system. Images of the surface were captured with a sampling rate of 15 Hz using the ARAMIS 2.3M camera system (GOM GmbH, Germany). With these pictures, the strain history during the deformation of the samples was computed based on the image correlation method. In accordance with DIN EN ISO 12004-2 (2009), the last picture before fracture was selected for evaluation. Major and minor strains are defined as the relative strains in the direction of the primary material axes. Following the DIN standard, where major strain is determined in the rolling direction of sheet metals, major strain was specified in the direction perpendicular to the grain for the VL, where higher strain was expected. Due to the different strain development of the VL in comparison to sheet metals, the conventional section-method for the determination of the forming limit curve (FLC) according to Bragard et al. (1972) could not be used. Therefore, the value of strain limit was evaluated in terms of major strain ($\varphi_1$) and minor strain ($\varphi_2$) directly at the point of crack initiation. Additionally, the major strain was picked as the average value over the whole captured strain field.

**Table 1** Results of Young's modulus $E_i$ and Poisson's ratio $\nu_{ij}$ given as mean value (coefficient of variation), n = 20

| Climate | Direction $i$ | $E_i$ (MPa) | $\nu_{ij}$ (–) | |
|---|---|---|---|---|
| N | 1 | 12,300 (42%) | $\nu_{12}$ | 0.4165 (34%) |
| | 2 | 900 (29%) | $\nu_{21}$ | 0.0305 |
| W | 1 | 6700 (38%) | $\nu_{12}$ | – |
| | 2 | 200 (17%) | $\nu_{21}$ | – |

**Table 2** Results of strength $\sigma_{max}$ and ultimate strain $\varepsilon_{max}$ given as mean value (coefficient of variation), n = 20

| Climate | Direction $i$ | $\sigma_{i,max}$ (MPa) | $\varepsilon_{i,max}$ (%) |
|---|---|---|---|
| N | 1 | 122 (49%) | 1.05 (26%) |
| | 2 | 11 (6%) | 1.84 (53%) |
| W | 1 | 65 (67%) | 1.01 (44%) |
| | 2 | 8 (6%) | 7.45 (5%) |

## 3 Results

### 3.1 2D tests

The results of the tensile tests are shown in Tables 1 and 2. A high anisotropy of the laminate can be proven. Under normal climate conditions, a Young's modulus ratio of perpendicular to parallel direction of 1:14 was found (Table 1). The ultimate strain was higher for the perpendicular direction. For this grain orientation, it was also observed that failure always occurred in the early wood

zone of the veneer. This behavior is owed to the low density and in particular the multitude of wide vessels of the ring-porous structure of ash wood (Wagenführ 2000). While this localization is homogenized for solid wood structures, these vessels have an effect of predetermined breaking points for thin wooden sheets such as veneers. The nonwoven backing cannot compensate this weakness.

The water treatment reduced stiffness and strength in both directions (Table 2). The ratio of anisotropy increased to 1:33 because the reduction of the Young´s modulus was higher in the transverse direction. At the same time, the tensile strength in the parallel direction was reduced to 50% under increased moisture but retained 70% in the orientation perpendicular to the grain. Ultimate strain, however, was not changed by high moisture content in the longitudinal direction but achieved a fourfold increase in the transverse direction.

Poisson's ratio at normal climate was determined from tensile tests in the parallel direction (Table 1). When the material was loaded perpendicular to the grain, however, the measured value of lateral strain was too low. This phenomenon is well known from literature (e.g., Niemz and Sonderegger 2018). The corresponding Poisson's ratio $\nu_{21}$ was calculated from the symmetry relation (Eq. 2). The variation in measured lateral strain was around 300% for samples tested after water pretreatment. Thus, no Poisson's ratios could be derived. The same difficulty for measurements above fiber saturation point was mentioned in Dietzel et al. (2016). The phenomenon was traced back to an opening and closing of microcracks. These quasi strains might have overlaid the lateral strain response of the sample. Microcracks could occur as a result of swelling.

Shear modulus was determined in the shear test with conditioned (20 °C/65% RH) and water-pretreated samples (Table 3). Shear strength and maximum shear strain, however, were only determined in normal climate conditions. Due to the limitation of the shear frame, shear stress could only be analyzed until 12% shear strain.

**Table 3** Results of shear modulus $G_{ij}$ and shear strain $\gamma_{max}$ given as mean value (coefficient of variation), n = 20

| Climate | Direction *ij* | $G_{ij}$ (MPa) | $\tau_{i,max}$ (MPa) | $\gamma_{i,max}$ (%) |
|---|---|---|---|---|
| N | 12 | 900 (9%) | 24 (12%) | 7 (21%) |
| W | 12 | 270 (12%) | > 10 (10%) | > 12 |

## 3.2 Failure surface

The Tsai–Wu failure hypothesis was applied to VL conditioned in normal climate and immersed in water. Measured strength values of tensile and shear strength were inserted into Eqs. 6–8, and a failure surface under plane stress conditions was calculated. Results are shown in Figs. 4 and 5. In case of decorative applications like surfaces of automotive trim parts, the material has failed when damage, i.e.

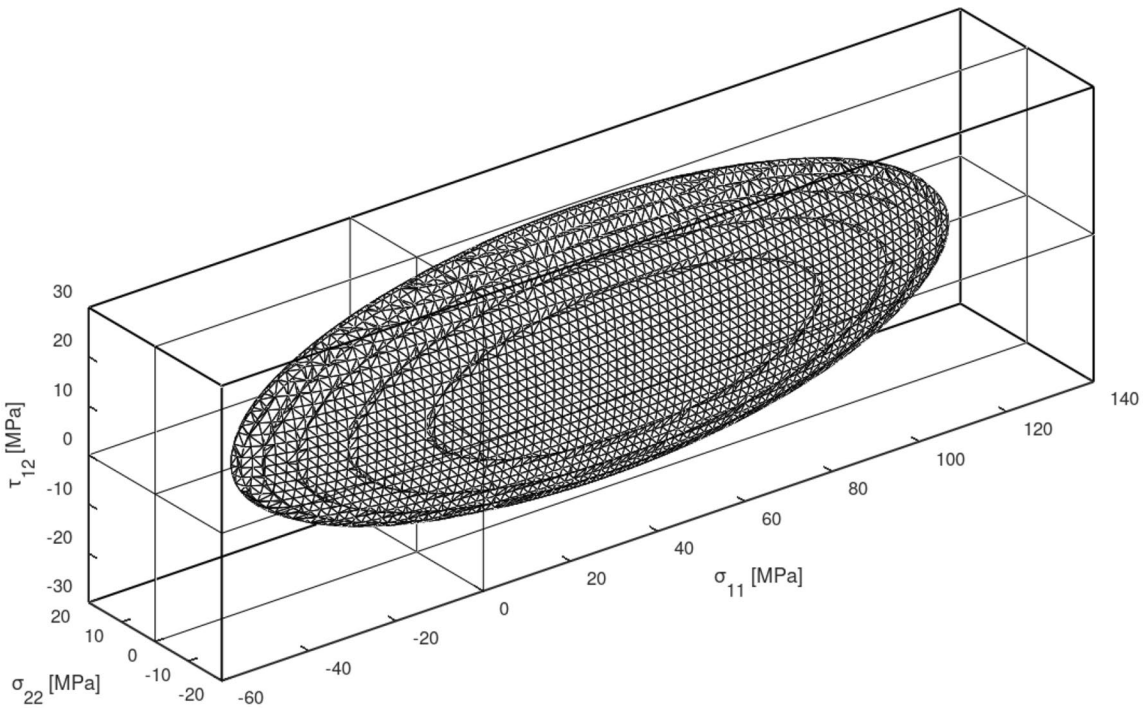


**Fig. 4** Tsai–Wu failure surface of ash wood VL at normal climate

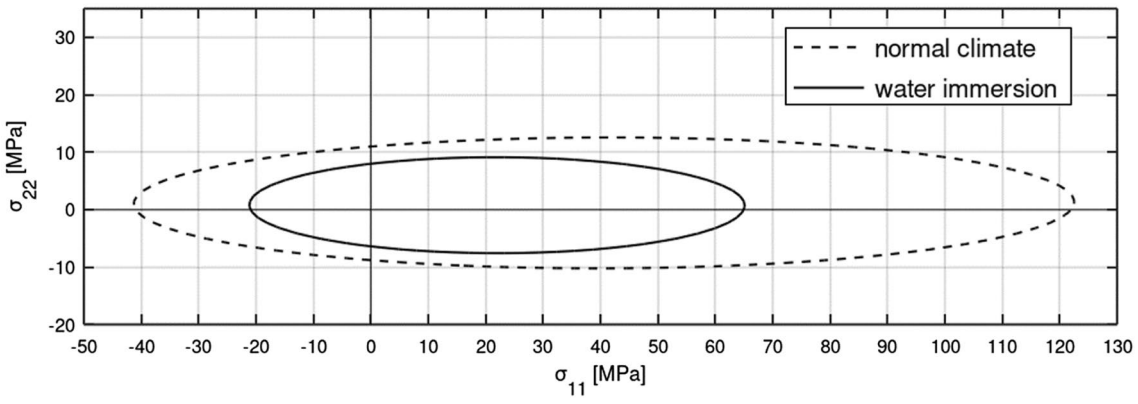


**Fig. 5** Tsai–Wu failure surface of ash wood VL at normal climate and after water immersion in the principal stress plane at $\tau_{12} = 0$

cracking, becomes visible. In tension, the point, where a crack is visibly open, matches with the maximum tensile strength. Under compressive loading, this point lies somewhere in the ductile range of the stress–strain curve. These states, where buckling effects and local distortions reach inacceptable limits, have to be defined from compression or forming tests. To complete the failure surface, compression strength was estimated based on the literature as starting value. Niemz and Sonderegger (2018) stated a ratio of 33% of compression strength to tensile strength in the longitudinal direction for common ash wood. In the radial and tangential directions, strength in compression is given there with 80% of the tensile strength. With the measured strength values given in Table 2 and based on these considerations, the strength parameters were calculated as (N: normal climate, W: water immersion):

$$f_{t,1,N} = 122\text{MPa}, f_{c,1,N} = 41\text{MPa},$$
$$f_{t,2,N} = 11\ \text{MPa},\ \ f_{c,2,N} = 9\text{MPa},$$
$$f_{s,12,N} = 24\text{MPa}.$$

$$f_{t,1,W} = 65\text{MPa},\ f_{c,1,W} = 21\text{MPa},$$
$$f_{t,2,W} = 8\text{MPa},\ f_{c,2,W} = 6\text{MPa},$$
$$f_{s,12,W} = 20\text{MPa}.$$

The interaction term $F_{12}$ was chosen very small with $2 \cdot 10^{-5}$ following Bellair (2013). Higher rotations lead to higher overestimations in the first quadrant of the principal stress diagram ($\sigma_{11} \geq 0, \sigma_{22} \geq 0$) for $F_{12} < 0$ or in the fourth quadrant ($\sigma_{11} \geq 0, \sigma_{22} \leq 0$) for $F_{12} > 0$ (Fig. 5). The exact value can be derived from fittings on biaxial measurements (Eberhardsteiner 2002).

The ellipsoidal failure surface intersects the principal stress axis at the specified strength limits. The asymmetry of strength in tension and compression causes an offset to the principal stress axis. This leads to small error assuming the highest stress limits in the main material directions. Apart from that, the Tsai–Wu failure surface captures the expected anisotropic failure behavior of VL between the strength limits adequately. Figure 5 shows the decrease in strength due to water immersion vividly.

### 3.3 Nakajima test

In standard Nakajima tests for sheet metals, usually a forming limit diagram is created. Based on points of major and minor strain, a forming limit curve (FLC) can be derived over the varying stress states. This curve describes the forming limit of a material, where all points above this curve mean material failure. In theory, it is expected that the minor strain is positive for biaxial stress in the S245 samples going to negative strain for uniaxial tension in the S30 samples (Fig. 6). This behavior was not verified. In the presented experiments, it was not possible to determine differences in the minor strain defined in the longitudinal direction (1) because of very low values until material failure. The

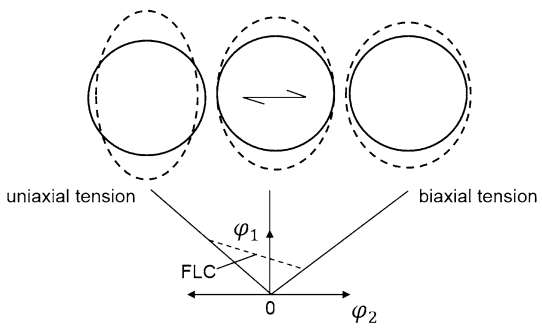


**Fig. 6** Expected deformation behavior and forming limit curve (FLC) for major strain ($\varphi_1$) and minor strain ($\varphi_2$) with the grain orientation in the horizontal direction

**Table 4** Results of punch way (z), global major strain ($\varphi_{1,global}$), local major strain ($\varphi_{1,local}$) until crack, with climates R (room climate), W (water immersion) and W + H (water immersion and heated tools), given as mean value (coefficient of variation), n = 10

| Climate | Parameter | Units | S245 | S125 | S70 | S30 |
|---|---|---|---|---|---|---|
| R | z | (mm) | 7.40 (3%) | 7.09 (4%) | 7.45 (4%) | 7.78 (2%) |
| | $\varphi_{1,global}$ | (–) | 0.011 (9%) | 0.010 (11%) | 0.011 (11%) | 0.013 (6%) |
| | $\varphi_{1,local}$ | (–) | 0.085 (39%) | 0.070 (22%) | 0.074 (33%) | 0.076 (19%) |
| W | z | (mm) | 16.25 (12%) | 17.05 (11%) | 18.62 (12%) | 17.84 (6%) |
| | $\varphi_{1,global}$ | (–) | 0.043 (16%) | 0.051 (21%) | 0.056 (15%) | 0.060 (20%) |
| | $\varphi_{1,local}$ | (–) | 0.174 (44%) | 0.226 (23%) | 0.227 (19%) | 0.242 (9%) |
| W + H | z | (mm) | 14.00 (12%) | 14.84 (3%) | 16.07 (3%) | 18.75 (6%) |
| | $\varphi_{1,global}$ | (–) | 0.045 (29%) | 0.056 (8%) | 0.060 (4%) | 0.063 (16%) |
| | $\varphi_{1,local}$ | (–) | 0.207 (39%) | 0.240 (13%) | 0.253 (8%) | 0.308 (20%) |

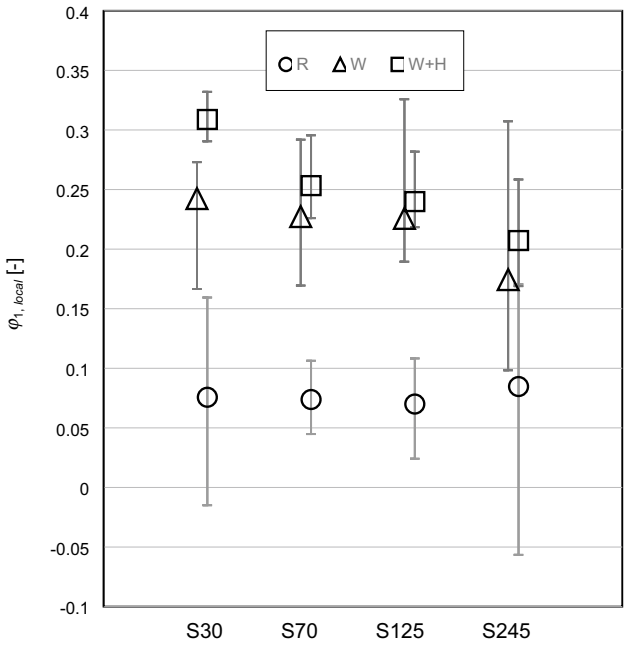


**Fig. 7** Major strain ($\varphi_{1,local}$) versus sample geometry with mean values, 95%- and 5%-quantiles, at room climate (R), after water immersion (W) and after water immersion with heated forming tools (W + H)

difficulty in the measurements of lateral strain in the direction parallel to the grain has already been discussed in the previous chapter.

However, a general difference in the forming behavior due to different stress states and different environmental conditions was found for the value of major strain. Due to relatively high variation in the results for the dry samples, no significant difference between varying geometries was found. Nevertheless, for water-immersed and combined water-immersed and heated samples major strain increased from S245 to S30 samples (Table 4, Fig. 7). This behavior is related to the anisotropy of the wood. In biaxial stress state of the S245 samples, the material flow is constricted through the stiffer longitudinal material direction. Higher straining was possible when the restraint of this direction was removed due to the sample geometry trimming. As a result, the samples S125, S70 and S30 could use their full capacity in perpendicular strain. Generally, major strain was much higher at the point of crack initiation compared to the value, which was taken globally from the entire strain field (Table 4).

The same effect of increasing major strain limit between S245 and S30 was observed from the global strain paths, given as a function of the punch movement as average of all individual curves (Fig. 8.). Initially, there is a sudden increase in the strain at the time of punch contact. This behavior is related to internal orientation effects like smoothening of the wavy surface. Subsequently, there is a linear increase in strain leading to high plastic deformation.

The Nakajima test showed clearly the expected superiority of combined heat and high moisture content during the forming process. The higher strain capacity of wood at elevated temperature and moisture is a well-known phenomenon for wood materials. The mild hydrolytic pulping of lignin and cellulose bonds in the cell wall leads to a softening effect, which generates higher deformation ability in the material (Goring 1963; Hillis and Rozsa 1978; Back and Salmen 1982; Irvine 1984).

The strain field analysis showed large local differences in the strain distribution over the VL sample (Figs. 9, 10). The major strain was mainly concentrated in the early wood zones. Failure of all samples occurred in an early wood zone with a crack propagation parallel to the grain. This behavior is related to the physical–chemical composition and the anatomical properties of the early wood. Early wood cells have thinner cell walls and larger lumens than late wood cell walls. Thus, there is less material to counteract outer forces. The local major strain limits even for the dry samples were much higher than the ultimate strain measured globally in the tensile test.

It has been observed that the crack did not always occur in the early wood zone closest to the center, where the highest material stress was expected due to the hemispherical stamp.

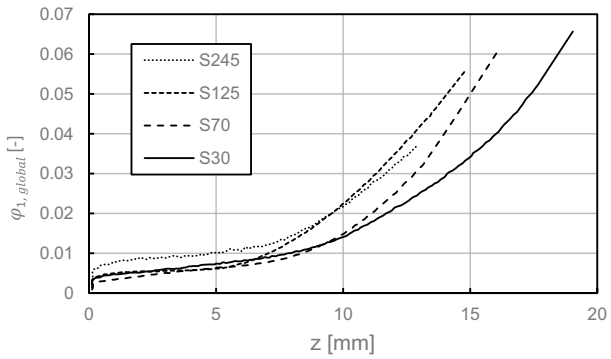


**Fig. 8** Major strain path ($\varphi_{1,\,global}$) vs. punch way (z) until visible crack for testing with heated forming tools and water immersed samples. Curves are the average of 10 individual curves per geometry

Moreover, the points for evaluating the maximum strain in the failing region were sometimes different from the points of highest strain inside the sample. This behavior is attributed to the inhomogeneity of the cellular wood structure.

## 4 Conclusion

For the characterization of the forming behavior of ash wood veneers with nonwoven backing (VL), tensile tests, shear tests and Nakajima tests were carried out. Basic constants for normal climate conditioned and water-immersed material were derived under the assumption of transverse isotropic material. The Tsai–Wu failure surface was applied to describe multidirectional strength of the VL. Significant differences in major strain at varying forming conditions were found from the Nakajima test. With heated forming tools and water-immersed material, the Nakajima test setup represents stresses under process conditions.

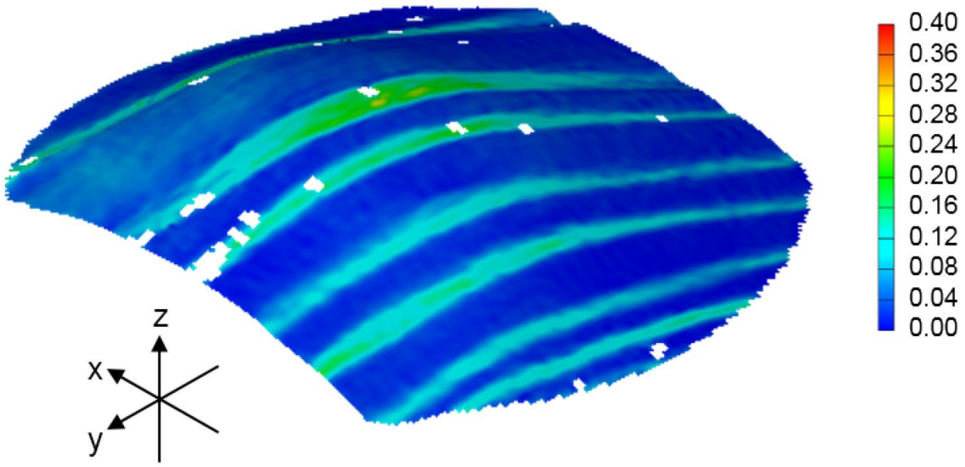


**Fig. 9** Major strain ($\varphi_1$) in sample S245 measured with digital image correlation

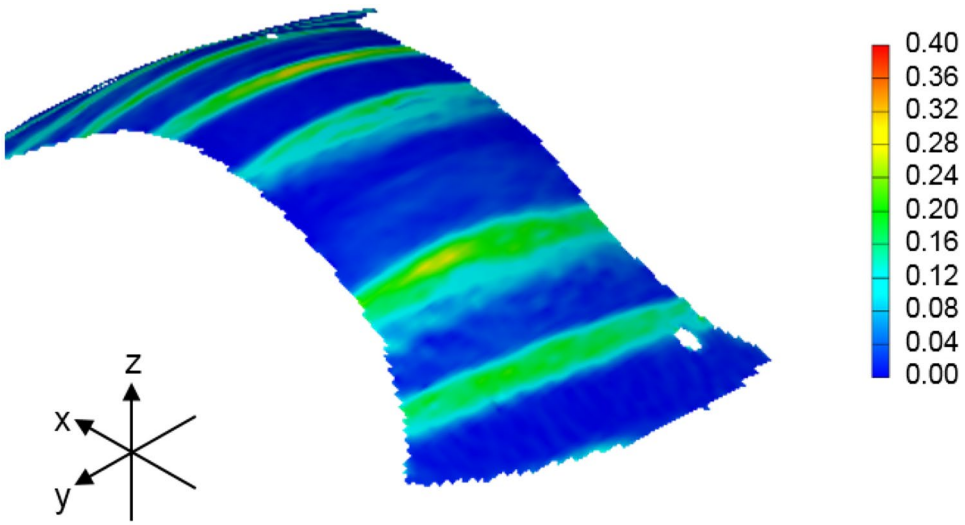


**Fig. 10** Major strain ($\varphi_1$) in sample S30 measured with digital image correlation

With the determined material parameters, the transverse isotropic material stiffness at normal climate is fully described. Measurements with water immersed samples can be used for material modelling with respect to forming simulations as an initial state, considering that water content is changing during the forming process under elevated temperature.

The Tsai–Wu failure surface captures anisotropic failure of VL's and predicts the load bearing capacity under different stress combinations. Furthermore, this criterion is available for many composite material models in libraries of common finite element software. Compression strength was estimated and has to be verified with further experiments.

The Nakajima test provides the opportunity to observe VL's in a forming scenario. Major strain limits and the failing behavior of VL's due to three-dimensional stress can be quantified. With water-immersed samples and heated forming tools an evaluation of the formability of thin VL sheets close to the real process conditions is possible. Due to the deformation of the sinking punch, the major strain was much higher in the early wood zones. In addition, the crack occurred in the early wood and propagated dependent on the cellular structure in the parallel grain direction. The constriction of the longitudinal material direction leads to lower strain limits in the hemispherical forming. In general, the forming limit perpendicular to the grain increased from biaxial to uniaxial stresses. Increased moisture and temperature caused a softening of the structure and resulted in higher formability. Highest forming degrees were possible with water-immersed material and forming tools heated to 140 °C, which is in accordance with forming parameters of the manufacturers.

The presented experiments contribute to the characterization of the VL forming process. The provided data can be used as input for numerical simulations. Besides the validation in simple standard tests, material models for forming simulations have to be validated on a 3D forming situation. Therefore, the Nakajima testing setup can be used to verify to what extent failure in different stress situations is captured from modelling approaches, like the Tsai–Wu criterion. Furthermore, finite element simulations could be used to predict and analyze the minor strain, which was not possible from measurements. With this method, the full forming limit diagram could be derived to assess the formability of VL's of different wood species.

**Acknowledgements** Open Access funding provided by Projekt DEAL.

## Compliance with ethical standards

**Conflict of interest** On behalf of all authors, the corresponding author states that there is no conflict of interest.



## References

Back EL, Salmen NL (1982) Glass transitions of wood components hold implications for molding and pulping processes TAPPI J 65(7):107–110

Bellair B (2013) Beschreibung des anisotropen Materialverhaltens von Rotbuchenfurnier als Basis für rechnergestützte Umformsimulationen (Description of the anisotropic material behavior of beech wood veneer as basis of numerical forming simulations). Zugl.: Ilmenau, Techn. Univ., Diss., 2012. Technische Mechanik. Shaker, Aachen

Bragard A, Baret J-C, Bonnarens H (1972) Simplified technique to determine the FLD on the onset of necking. C R M 33:53–63

Buchelt B, Wagenführ A (2010) Influence of the adhesive layer on the mechanical properties of thin veneer-based composite materials. Eur J Wood Prod 68(4):475–477

Chanda A, Bhattacharyya D (2018) Formability of wood veneers: a parametric approach for understanding some manufacturing issues. Holzforschung 72(10):881–887

Clauß S, Pescatore C, Niemz P (2014) Anisotropic elastic properties of common ash (*Fraxinus excelsior* L.). Holzforschung 68(8):941–949

Dexle C, Wiblishauser M (1999) Patent: Furniersystem hoher Flexibilität und Verfahren zur Herstellung eines solchen DE19803262 A1, 05.08.1999 (backing material for laminations)

Dietzel A, Raßbach H, Krichenbauer R (2016) Material testing of decorative veneers and different approaches for structural-mechanical modelling: walnut burl wood and multilaminar wood veneer. BioResources 11(3):7431–7450

DIN EN ISO 12004-2 (2009) 02 Metallic materials—sheet and strip—determination of forming-limit curves—part 2: determination of forming-limit curves in the laboratory (ISO 12004-2:2008)

Eberhardsteiner J (2002) Mechanisches Verhalten von Fichtenholz (mechanical behavior of spruce wood). Springer Vienna, Vienna

Fekiac J, Gáborík J, Smidriaková M (2016) 3D formability of moistened and steamed veneers. Acta Facultatis Xylologiae Zvolen res Publica Slovaca 58(2):15–26

Fekiač J, Zemiar J, Gaff M, Gáborík M, Marušák R (2014) 3D-moldability of veneers plasticized with water and ammonia. BioResources 10(1):866–876

Franke T, Herold N, Buchelt B, Pfriem A (2018) The potential of phenol–formaldehyde as plasticizing agent for moulding applications of wood veneer: two-dimensional and three-dimensional moulding. Eur J Wood Prod 76(5):1409–1416

Goring DAI (1963) Thermal softening of lignin, hemicellulose and cellulose. Pulp Paper Mag Can 64(12):T517–T527

Goswami L, Eder M, Gierlinger N, Burgert I (2008) Inducing large deformation in wood cell walls by enzymatic modification. J Mater Sci 43(4):1286–1291

Grabner M, Wolf A, Schwabl E, Schickhofer G (2016) Methods of forming veneer structures. In: World conference on timber engineering, 22–25 Aug 2016 Vienna, pp 849–858

Herold N, Pfriem A (2013) Impregnation of veneer with furfuryl alcohol for an improved plasticization and moulding. Holz Roh Werkst 71(2):281–282

Hillis WE, Rozsa AN (1978) the softening temperatures of wood. Holzforschung 32(2):68–73

Irvine GM (1984) The glass transitions of lignin and hemicellulose and their measurement by differential thermal analysis. TAPPI J 67:118–121

Krüger R, Buchelt B, Wagenführ A (2018) New method for determination of shear properties of wood. Wood Sci Technol 52(6):1555–1568

Mascia NT, Simoni RA (2013) Analysis of failure criteria applied to wood. Eng Fail Anal 35:703–712

Nakajima K, Kikuma T, Hasuka K (1968) Study on the formability of steel sheets Yawata. Tech. Rep., Kyoto, pp 8517–8530

Navi P, Sandberg D (2012) Thermo-hydro-mechanical processing of wood, 1st edn. EPFL Press, CRC Press, Lausanne, Boca Raton

Niemz P, Sonderegger WU (2018) Holzphysik: Physik des Holzes und der Holzwerkstoffe (Physics of wood and wood products). Carl Hanser Verlag GmbH & Company KG (2018)

Pfriem A, Buchelt B (2011) Influence of the slicing technique on mechanical properties of the produced veneer. Eur J Wood Prod 69(1):93–99

Srinivasan N, Bhattacharyya D, Jayaraman K (2007) Thermoforming of wood veneer composite sheets. Holzforschung 61(5):224

Tsai SW, Wu EM (1971) A general theory of strength for anisotropic materials. J Compos Mater 5(1):58–80

Wagenführ R (2000) Holzatlas (Wood atlas), 5th edn. Fachbuchverl. Leipzig im Hanser-Verl., Leipzig u.a., Wien

Wagenführ A, Buchelt B, Pfriem A (2006) Material behaviour of veneer during multidimensional moulding. Holz Roh Werkst 64(2):83–89

Zerbst D, Clauss S (2018) Patent: Verfahren zum Herstellen eines Furniersystems mit erhöhtem Formänderungsvermögen, insbesondere für ein Holzzierteil im Fahrzeuginnenraum, sowie Furniersystem DE102018002709, 27.09.2018 (veneer system with improved forming properties for decorative trim parts in the car interior)